

THESEUS

T-Tauri & HErbig Ae/Be stars Study with Echelle Uv Spectrograph

Team Orange

July 28th, 2011

Abstract

THESEUS is a proposed space based mission to study medium and low mass, pre - main sequence stars in the ultraviolet wavelength range. This mission shall gain knowledge of this short but critical period of stellar formation and reveal current unknowns involving turbulence, magnetic fields, and angular momentum. These phenomena will be observed via their effects on the UV emission lines with a high and medium resolution spectrographs together with polarimetric measurements of the continuum. An observational target list of more than 600 objects will be sampled from a quasi-Halo orbit around L2 over a period of 5 years, spanning all of their known variability time scales.

1 Scientific Background

A key goal in astronomy is to study and fully understand the complex process of star formation. One of the important stages of star formation is the pre-main sequence stage, or the period between the initial birth of a protostar and becoming a main sequence star. This stage is characterised by dynamical jets, protoplanetary accretion disks, strong magnetic fields, and turbulence. These different processes can only be studied on a broad range of wavelengths, including IR, VIS, UV and X-ray.

Pre-main sequence stars are one of the best candidates to study star formation since they are in most cases already visible in the visual range (Class II and III stars).

The main types of pre-main sequence stars are low mass T Tauri stars, characterised with a mass $M < 2 M_{\odot}$, and intermediate mass Herbig Ae/Be stars, characterised with a mass $2 M_{\odot} < M < 8 M_{\odot}$ (Ward-Thompson & Whitworth 2011). Higher mass protostars are more than likely not observed due to shorter transition times to main sequence. Both T Tauri stars and Herbig Ae/Be have highly active environments. Their magnetic fields, observed at roughly order of kG (Errico et al., 2001), are thought to be the result of

deuterium burning that thermally drives the differential rotation of the protostar (Shu et al. 1987).

The strong magnetic fields have other effects on the accretion process and overall brightness of the protostar. Lynden-Bell & Pringle (1974) pointed out more than 30 years ago that the accretion disk is an important source of excess emission of T Tauri stars, specifically IR emission from the outer disk and UV emission from the boundary layer where disk material in quasi-Keplerian rotation settles down on the slowly rotating stellar surface. In more recent models, the accretion disk seems to be disrupted at a few stellar radii by the stellar magnetic field, and the material falls along the field lines at nearly free-fall velocity. The evidence for magnetospheric accretion is based mainly on three observational properties: (1) the broad emission lines, often with redshifted absorption components, are consistent with emission from infalling gas channeled by the magneto-sphere (Calvet & Hartmann 1992; Hartmann, Hewett, & Calvet 1994; Muzerolle, Calvet, & Hartmann 1998; Muzerolle, Hartmann, & Calvet 1998a, 1998b); (2) the near-IR colours and spectral energy distributions (SED) of classical T Tauri stars (CTTS) indicate emission from disks that is truncated at a few stellar radii (Kenyon et al., 1994; Meyer, Calvet, & Hillenbrand 1997); (3) one of the three distinct types of variability displayed by CTTS (type II variations) can be interpreted as emission from hot spots on the stellar surface where infalling material impacts the star (Herbst, Herbst & Grossman 1994, and reference therein; Gullbring et al., 1996).

2 Mission Objectives

2.1 Main Objectives

This mission (THESEUS) is the first mission to integrate the study of a wide range of aspects of pre-main sequence stars, including the chromosphere and corona, magnetic fields, turbulence, jets, and accretion disks, in an extensive list of T Tauri and Herbig Ae/Be stars in the ultraviolet wavelength range. It is

necessary to observe these pre-main sequence stars in the UV in order to probe hot ionised gas in the chromosphere that we are unable to study in IR or optical wavelengths and directly relate the observed ionised gas to the magnetic fields produced. It is equally important to study the inner accretion disk and stellar jets in the UV range for similar reasons. More specifically, this mission will answer the following questions:

- How does the magnetic field correspond to the overall brightness and the change in flux of spectral lines of T Tauri and Herbig Ae/Be stars and do the variations relate to hot spots on the stellar surface?
- What are the effects of magnetic fields and turbulence on accretion and planetary formation?
- What aspects of T Tauri and Herbig Ae/Be stars are time dependent?
- How does the loss of angular momentum occur during the pre-main sequence star formation?
- How do stellar jets affect the medium surrounding the pre-main sequence star?
- Can we relate observations from T Tauri and Herbig Ae/Be stars to current theories of chromospheric activity involving the Sun?

2.1.1 Outer Atmosphere of T Tauri Stars and Herbig Ae/Be Stars

Pre-main sequence stars have chromospheres with observable emission lines that can only be studied in the UV wavelength range. The strongest of these lines are the Mg II h and k doublets (2796 Å and 2803 Å), but C IV (1548 Å) and Si IV (1403 Å) are also strong at ambient temperatures near 10^5 K (Stahler & Palla, 2004). Using these ions quite common in the T Tauri and Herbig Ae/Be stars, we can calculate temperatures from their atmospheres. If high resolution spectroscopy is used to observe the emission lines, Zeeman splitting or broadening can also be related to the corresponding magnetic field of the observed region, which is typically around 1 kG in T Tauri and Herbig Ae/Be stars. Therefore, variations found in both the temperature and magnetic fields of T Tauri and Herbig Ae/Be stars over a time period of days to several weeks can be studied and potentially related to hot spots in the stellar atmosphere (Daou & Johns-Krull, 2006).

2.1.2 Magneto-Rotational Instability

A key question in star formation is the significance of the interaction between the stellar magnetic field, the

circumstellar disk, and bipolar jets, discussed in Section 1. Disk accretion and stellar jets are the result of turbulence caused from magneto-rotational instability (MRI). The jets are optimally traced in the UV wavelength range, typically from semi-forbidden ions O III]₁₆₆₅, C III]_{1907,1909} and Si III]_{1883,1892}. Not only can the temperature be calculated from the spectral lines, but the intensity ratio between C III] and Si III] is sensitive to the gas particle densities and can be used to estimate the electron densities with a range of $10^8 \leq N_e \leq 10^{13}$ cm⁻³, which are also observed in late-type stars. However, these lines are also produced in hot pre-shock regions with $T \sim 10^6$ K. These shock fronts are produced by material accreting onto the stellar surface, where the semi-forbidden lines are expected to form in regions where X-ray radiation (resulting from the post-shock regions) ionises the infalling gas (Gomez de Castro, Verdugo, & Ferro-Fontan 2003). In addition to the densities, the flux ratio of the lines can be related to the velocity of infalling gas from the accretion disk as well as the jet velocity of the pre-main sequence star. Combined with information about stellar dimension, the energy flux of the accretion flow and accretion luminosity can be derived (Errico, Lamzin, & Vittone, 2001).

The information in the ultraviolet range of the semi-forbidden lines can be used to calculate the temperature. The line broadening yields the velocity and densities of the jets and the accreting regions. Combined with polarimetric data that determines the direction of the magnetic field in the protostellar region, the relation between the magnetic field, temperature, velocities, and densities of the stellar jets and accretion can be studied.

2.1.3 Time Variability

As mentioned in Sections 2.1.1 & 2.1.2, pre-main sequence stars are located in dynamical environments that can vary greatly over many timescales. Studying a wide range of T Tauri and Herbig Ae/Be stars over equal periods of time would give a more complete view of their irregular evolution on short time scales of up to five years.

2.1.4 Disk Inclination

The circumstellar disk is rich in mainly dusty material that polarises scattered light. Using polarimetry measurements, this can be used to infer the inclination of the circumstellar disk (Clemens 2010). A disk that is face-on has a polarisation that is equal across the disk. A disk that is edge-on has a polarisation that differs from the front to the back edge. Disk inclination,

Table 1: List of scientific requirements for THESEUS.

Wavelength Range:	110–310 nm
Field of View:	10'' minimum
Angular Resolution:	0.1''
Spectral Resolution:	100,000 (optimal resolution) 15,000 (minimum resolution)
Limiting Magnitude:	17 mag
Observational Time:	5 years +

combined with the magnetic field and velocity measurements, will also permit us to have a better idea of the overall environment of the pre-main sequence star.

2.2 Additional Potential Objectives

This mission can also be applied to other areas of research. From the UV spectral features of CO ($\lambda > 1560 \text{ \AA}$) present in the inner regions of warm inner circumstellar disk, we can infer a CO column density and rotational excitation temperature. Combining these results with work on photo- and collisionally excited H₂ emission, we can show how the relative density of CO/H₂ evolved between the much lower interstellar value and the higher value observed in solar systems and comets today (France 2011).

Observations of the line and continuum emission combined from collisionally excited H₂ and from accretion shocks can constrain the physical properties of the emitting region. This can solve outstanding issues concerning how the attenuation processes operate in protostellar disks, including the effective temperature and absolute strength of the ratio found in low mass protoplanetary environments (France 2011). Polarimetric techniques can be used for direct detection of starlight that is scattered in a planetary atmosphere. Therefore, we would infer its orbital period, the inclination, eccentricity, and orientation of the orbit as well as the nature of scattering particles in the planetary atmosphere (Berdyugina, 2001).

On the extragalactic scale, the feasibility of using the Mg II line for reverberation mapping of high-luminosity quasars at intermediate redshift, $0.4 \leq z \leq 0.6$, has been demonstrated by Woo 2008. In addition, a recent survey of long duration gamma ray bursts at $z = 1.1$ has shown contradictions with current models for the population and type of extinguishing sources along the lines of sight. Further observations are necessary to develop and refine the models (Prochter, 2006).

Table 2: Minimum chromospheric magnetic field detectable at $R = 100000$.

Line (\AA)	B (kG)
Mg II h 2803	3
Mg II k 2796	1.3

3 Scientific Requirements

3.1 Wavelength Range

The wavelength range for our proposed mission is the near-UV (NUV) & far-UV (FUV) from wavelengths 120–320 nm. This wavelength range allows us to see the most prominent ions in the chromosphere of T Tauri and Herbig Ae/Be stars (Mg II h & k, C IV, and Si IV) as well as semi-forbidden ions originating in stellar jets and accretion disks (O III], C III], and Si III]).

3.2 Field of View & Angular Resolution

The field of view at 10'' is based on one of the nearest molecular clouds with known T Tauri and Herbig Ae/Be stars in the Gould Belt, Taurus (explained further in Section 3.4). It is at a distance of 140 pc from Earth (Errico, Lamzin, Vittone 2001). Even though the average radius of an accretion disk is 100 AU, it can have a diameter of $\sim 1000 \text{ AU}$ (D'Alessio et al 1999). The field of view is based on our ability to observe UV light scattered of a large accretion disk at a distance of Taurus.

3.3 Spectral Resolution

Three spectral resolutions are used. The high resolution in the wavelength range of 250–310 \AA is needed to resolve the Zeeman splitting or broadening of the strongest lines observed in the chromosphere of the pre-main sequence star (Mg II h & k). This yields the strength of the magnetic field (See Tab.2). Medium resolution, $R \sim 15,000$, allows us to span the entire wavelength range of 1200–3200 \AA . We can resolve all of the permitted and semi-forbidden lines we need to study the chromosphere, accretion disk, and stellar jet. In order to measure the polarisation of light, a polarimeter requires a coarse spectrum with very low resolution of $R \sim 330$. The polarisation of light can be used to calculate the magnetic field direction from the flux, the linearly polarised spectrum, and the polarisation angle as a function of wavelength.

3.4 Observational Lifetime

The observational lifetime of the telescope is expected to be at least 5 years in order to observe a composed catalog of (500) T Tauri and (100) Herbig Ae/Be stars over timescales long enough to observe different variability regimes. The relatively permissive thermal requirements and the usage of UV wavelength, imply the solar aspect angle restriction to be only 45 away from the Sun, thus allowing for light constraints on the observational strategy. The frequency of observations will depend on the density of targets in different regions of the sky, yielding a representative sample that will allow to perform the desired statistics on the above mentioned variability time-scales.

4 Telescope Design

4.1 Telescope Choice

To get a high spatial resolution of 0.1" the natural choice will go toward the Ritchey Chretien Telescope which is aplanatic and so it is designed to eliminate the spherical aberration and the coma.

4.1.1 Telescope Calculations

First we did calculate the focal length of the equivalent lens using a simple triangle calculation with the given sizes of the Field of View and the size of the MCP detector (see Figure 1). The focal length of our system is then 10.8 m. After this simple calculation, we have to determine the position of our secondary mirror. Before this calculation we decide to put our imaging instrumentation at 80 cm behind the primary mirror. This position is the position of the focus of our system. A geometrical calculation of the light path can give us a rough position of our secondary mirror. This gives us an approximate position of 1.35 m from M1. We must first check that the curvature of the mirrors is feasible. ($D = 1.35$, $B = 2.15$, $F = 10.8$). The respective curvatures for M1 and M2 are: 3.37 m and 0.8 m which are feasible (15cm deviation at the tip for M1). We can now check that our system correspond to the wanted system. The image (O') of an infinite object (O) seen by the primary mirror will be on its focus plan ($F1$). The image (O'') of this image (O') by the secondary mirror will have then to be positioned on the focus of the optical system (F). Having these information we can easily determine the focal lengths of our mirrors.

4.1.2 Telescope Structures

Now we have all the measurements of our telescope we can start to "dress" it up! The Mirrors will be done

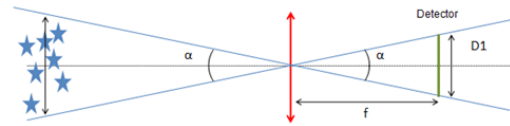


Figure 1: focal length calculation

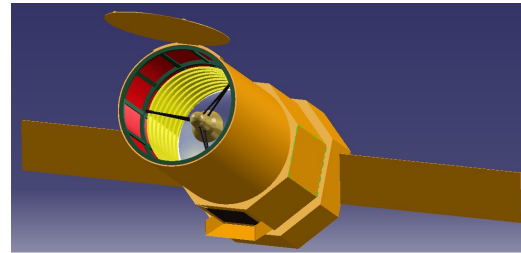


Figure 2: Impression of the satellite

in Silicon Carbide. This material has been chosen due to its thermal properties (e.g. thermal expansion coefficient $2.0 \cdot 10^{-6}$ at room temperature and below 150K) and its density (2.7). The primary mirror consists in 18 segments assembled together, coated with 150 nm of Al and MgF_2 for UV sensitivity using the CVD process and polished into a single hyperbolic surface of 12 mm (done on Herschel) with a roughness inferior to 1 nm RMS ($< 1/10$ th of our lowest wavelength). The Secondary mirror a single 40 cm mirror made in the same material and manufactured the same way as the primary. The mounting is a 5 points frame made in Carbone Fibre chosen for its lightness and strength. The Secondary mirror mounting consists in a 3 points frame made also in Carbone Fibre. The Baffles are made in Aluminum. The Main Baffle is 2.21 m diameter. The Telescope main structure is also made in Carbone Fibre and consists in 4 rings linked together by 9 graphite tubes.

4.2 Instruments

4.2.1 High Resolution Spectrograph

As mentioned above one very important science objective is to investigate the magnetic fields of pre-main-sequence stars. In order to obtain measurements of these fields we like to observe the spacing of several lines ($Mg II$; $C IV$) and line broadening due to Zeeman splitting. For this part of our project we will use a central wavelength of 280 nm ($MgII$) and need a dispersion of 0.0014 nm/pix which leads to a required resolution of the spectrograph of at least $R=100,000$. Because of a given detector size of 4000 x 4000 pixels we propose an Echelle spectrograph to fulfill our requirements.

The advantage of such an spectrograph is the achievement of very high resolution and a broad

wavelength range. furthermore it leads to a compact size and big throughput of light in comparison to conventional spectrographs with similar resolution (Schroeder et al. 1970).

There are two general possibilities to achieve a high resolution with a grating spectrograph. One is to enlarge the illuminated grooves of the used grating. Since the resolution is directly proportional to the diffraction order, the other one is to go to higher diffraction orders.

Using an echelle grating as blaze grating it is feasible to shift the maximum throughput of light to an high order and achieve a high resolution with minor losses. At high diffraction orders all the spectra are overlapping. So a cross dispersion element is typically used to separate them on the detector. With this design the complete detector can be used to get the complete spectral range from 2500 Å- 3200 Å.

In this spectrograph a silica glas prism will be used as cross dispersing element. The advantage of using it is a better resolution especially for the short wavelength-range in comparison to a grating.

4.2.2 Medium Resolution Spectrograph

To get medium resolution spectra with a long spectral range we propose to use a lightweight version of the STIS Instrument which is currently mounted on-board the Hubble Space telescope. To reach the broad wavelength range from 1640Å-3100Å we propose a long slit spectrograph wich is using a first order grating with a 1024 pix detector and gives a spectral resolution of 0.09 Å/pix ($R = 9110 - 17220$). With one single exposure a spectral range of 90 Å will be covered. The grating will be scanned in 18 single exposures in order to reach the full spectral coverage. While using a prismwheel it will be possible to put an other first order grating into the light path. So with the 1024 pix detector we can cover a wavelenth range of 55 Å in one exposure. To reach the complete wavelength range from 1140Å to 1740Å (with $R = 11400 - 17400$) the grating will scan in 12 exposures similar to the other grating. For wavelength calibration a internal calibration lamp will be used. Using a modified version of this space qualified instrument with two different gratings leads to lower costs and will fullfill perfectly our needs.

4.2.3 Spectro-Polarimeter

For investigations regarding the direction of the magnetic field we propose a spectro-polarimeter which adoptes the principle design of the WUPPE spectro-polarimeter. With this instrument it is possible to obtain low resolution ($R = 330$) spectra that will give us

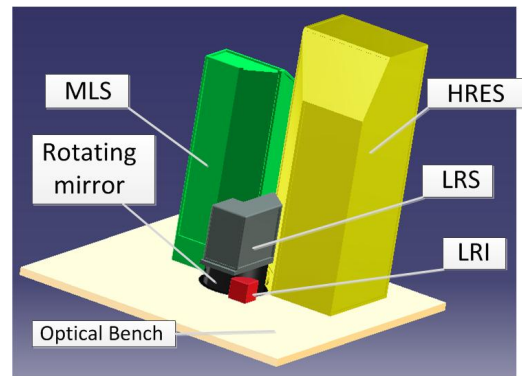


Figure 3: Layout of our instruments on the optical bench

informations about polarisation - angle and intensity. The instrument is a modyfied Monk-Gillieson Spectrometer.

After passing the slit the light will pass through a Wollaston polarizing beam-splitter. This is a birefringent polarizer which consists of two magnesium fluoride prisms. These prisms will be able to split the light into two orthogonal-polarisation directions. Using a grating we obtain low resolution spectra of both components simulaniously. Furthermore we will use as detectors two linear MCP detector-arrays with 1024 pix. To measure the polarisation on specific points of our target with different disc sizes we add a Variable aperture wheel with Apertures form 2" to 10". The advantage of this instrument is the broad wavelength range from 1400 Å to 3200 Å and the adopting of space tested components.

4.2.4 Imager

For imaging and photometric measurements a low resolution imaging device will be needed.

It will be mounted in the focal plane and able to project the 10" field of view with a resolution of at least 0.1" pix. The used MCP-detector will have a size 300 x 300 pix and will be coated for a high sensitivity in FUV, but less sensitive in the optical spectral range. So we can be sure to drop visual- and IR-light.

4.2.5 Instrumentation Configuration

HRES (High Resolution Echelle Spectrograph) , LRI (Low Resolution Imager) and MLS (Mid resolution Long slit Spectrograph) are positioned around the rotating mirror, which distributes the light beam into those instruments. The Spectropolarimeter (LRS) is installed on the top of Rotating Mirror. Everything is fixed on the Optical Bench surface, which is hollow in the middle.

4.2.6 Ultraviolet detectors

Quantum efficiency of normal CCD detectors is very low for small wavelength making them very inefficient at detecting ultraviolet photons. Also there is a cutoff wavelength below which no photons can be detected. So other technologies have been invented. UV detectors and Microchannel plates (MCP) are two of them. However most standard UV detectors are solar blind. We cannot use such detectors as they block exactly the wavelengths we want to measure. Chandra is using MCP technology to detect x-ray photons and WSO is planning to do so for UV photons. So we are proposing to use MCP too. In fact, MCP is best suited for detecting vacuum ultraviolet (< 200 nm) radiation and medium to near UV rays (< 320 nm) at the same time. Also the lifetime of MCP detectors is suitable for our mission. A test of MCP lifetime has been done with the Cosmic Origins Spectrograph onboard HST. It says that with minimal flat fielding detective quantum efficiency of the MCP should not decrease by more than 1% for a fluence of 10^{11} photons/cm² (Wilkinson E. 1999).

MCP is a 2D sensor that detects UV photons through production of photoelectrons and amplifies the detected signal. It consists of a plate with many channels. When a photon hits the coated inner layer of a channel an electron is produced that travels towards anode as a potential gradient is applied from cathode to anode. More and more electrons are produced as they hit opposing walls. All these electrons are collected at the anode side by multi-anode charge-collectors. The channels are a bit bent so that electrons cannot bounce back.

Following HRC-I instrument of Chandra we use wires as multi-anode. A group of wires is connected to one charge-sensitive amplifier that supplies the detected charge to an analog to digital converter.

Size of one group of wires connected to an amplifier determines our pixel size. We take this size to be comparable to the pitch of the MCP. We did not find any MCP in the market that we can use. So we propose to order MCP with required specifications. We need 3 detectors for 3 different instruments. Our general specifications are:

- Quantum efficiency: 40-50%
- Inner layer coating: NiCr+Cs-Te+CuI+MgF₂ (Cs-Te and MgF₂ together make the MCP sensitive to 110-310 nm wavelength)
- Dark current: 3 cts/s/cm²
- Gain: 10^7

- Channel length-diameter ratio - 60:1
- Stages: 2

5 Critical Technologies

This mission requires numerous critical technologies that must function to the specified requirements or the mission will not be considered a success. The Technology Readiness Levels (TRL), documented by ESA, provide a metric in which the feasibility and complexity of each component of the space craft and payload design can be measured. Some key technologies with lower TRL values are shown in Table 3. The primary mirror is a very critical technology. Since we are observing in the UV wavelength range, the smoothness of the mirror must be incredibly precise ($< \frac{1}{10}\lambda$). In addition, the configuration of 18 separate pieces being polished into one parabolic surface has only been used with Herschel, which observed in the FIR and requires less surface smoothness. For these reasons, we have assigned a TRL of 3 to the primary mirror. Other high TRL items are the Echelle Spectrograph, since we have to redesign the grating, and the Spectropolarimeter, since we are

6 Spacecraft Design

6.1 Method

Concurrent engineering design was applied in the design of the spacecraft and involved utilising an integrated spacecraft model of all the individual subsystems which are linked. This was achieved through linked Excel spread sheets synced in an iterative process. This enabled the design engineers to work concurrently and allowed the spacecraft design to adapt to changing and developing requirements imposed by the payload.

6.2 Driving System Requirements

Driving system requirements were identified at early stage of the project and included: Observational strategy requirements including constraints on the Sun Spacecraft and Earth Spacecraft Angle as well as the requirement to be able to observe targets in the Gould Belt, which is inclined to the ecliptic; High pointing requirements of 0.5" accuracy and 0.25"/h stability; stringent thermal requirements on the detector plane instruments; and the physical dimensions of the telescope structure.

6.3 Mission Analysis

Since the spectrum to be investigated lies within the UV spectrum the observation must be done from space. In order to fulfil both the scientific objectives and the payload requirements several types of orbits, including SSO (Sun Synchronous Orbit), HEO (Highly Elliptical Orbit) and orbits around the Lagrangian point, L_2 , have been taken into consideration. Orbits around L_2 have already been successfully used for space observations in the past (Herschel, Planck, Gaia), and will serve the JWST in the future. Driven by the fact that the large majority of targets to be observed lie within the Gould Belt, which is tilted toward the galactic plane by about 16 to 20 degrees, and based on requirements, such as the visual constraints and thermal stability, an analysis yielded that both a Quasi-Halo orbit around the L_2 and a SSO would principally meet the mission's requirements. However, we selected a Quasi-Halo orbit, which has the major advantages of

- a better and easier observational strategy with respect to observational time and variety of observable targets at specific points in time, and
- a much lower delta-v budget, since the delta-v required for orbit insertion is small ($\approx 8.7\text{m/s}$), the orbit maintenance is cheap (10-20m/s every 4-6 months), and there is no disposal needed (unstable orbit).

The only reasonable choice for the launcher is the Soyuz-Fregat-2B with launch from Kourou. The satellite dimensions of approximately 5.6m length, 2.7m total diameter and 2.4m telescope diameter, and the total wet mass of 2128kg (incl. margin) meet the usable volume and mass limitation (2150kg), respectively, that can be carried to L_2 by this Soyuz model. Due to the total length of the S/C a dual launch to SSO, what would considerably reduce the costs, is not possible in the current configuration.

6.4 Systems Level

Mass Budget. A system level mass budget is shown in Figure 4. Component level margins were applied to all components based on the Technology Readiness Level (TRL) of the component, with high TRLs receiving a 5% margin, medium TRLs a 10% margin and low TRLs a 20% margin. A system level mass margin was applied of 20%. Some assumptions were made with regards to the mass of the structure and of the harness, with 20% and 2% of dry mass respectively being assumed. The payload makes up approximately

60% of the mass of spacecraft and this payload fraction is consistent with previous missions and provides some verification.

System	Mass without Component Margins	Mass With Component Margins
AOCS	100	111
Comms	29	35
Power	85	94
Propulsion	38	43
Payload	898	1008
OBDH	50	52
Environment/Thermal	31	37
Harness	21	23
Structure	300	315
Total Dry Mass	1551	1717
System Margin (20%)	310	343
Propellant/Consumables	67	67
Total Wet Mass	1928	2128

Figure 4: System level mass budget.

Power Budget. Figure 5 shows the power budget for the various mission modes in which the spacecraft can operate. The mode with highest power requirement and hence the driving requirement is that observational mode during only one of the four instruments is operating at any time.

Mode	1	2	3	4
Mission Phase Subsystem	Deployment/Early Ops	Observation Mode	Manoeuvring Mode	Caretaking/Downlinking
AOCS	340	340	340	340
Power	0	0	0	0
Comms	63	0	63	63
Propulsion	274	0	274	0
OBDH	30	225	30	225
Environment/Thermal	164	164	164	164
Harness	0	0	0	0
Payload	0	324	0	0
Subsystems Total (W)	871	1053	871	792
System Margin	174	211	174	158
Total Power (W)	1046	1263	1046	951

Figure 5: Power budget for the various mission modes.

6.5 Configuration

The configuration of the spacecraft is split into three main sections: the telescope module, the instrument

module and the service module. Figure 2 shows a CAD model of the spacecraft. The solar arrays and communications systems are located on the service module while the radiator is located on the instrument module with a sun shield in order to provide cooling.

6.6 AOCS and Propulsion

Mainly driven by the requirements of 0.5" pointing accuracy with 0.25"/h pointing stability the following components form the attitude and orbit control system. High accuracy is achieved by fine pointing sensors and there are four off the shelf reaction wheels, from which one is redundant. 2 star trackers, 3 Sun sensors, 3 guidance sensors, 2 inertial measurement units and two attitude control computers are both necessary and sufficient for station keeping and pointing.

The low delta-v requirements of $\approx 8.7\text{m/s}$ for orbit insertion and $\approx 10\text{-}20\text{m/s}$ every 4-6 months yields an all-in-all propellant mass of $\approx 50\text{kg}$, where a simple mono propellant MMH system is chosen. 12 thrusters clustered in 4 groups of each 3 guarantee S/C movability in each direction. The same thrusters are used for orbit correction and angular momentum management. Moreover, redundancy in thrusters, piping and valves are considered for risk mitigation. Two mono propellant tanks, piping, control electronics, filters and drain valves completes the propulsion subsystem.

6.7 Thermal Control Subsystem

The major heat load in the thermal environment around the L_2 is the radial thermal energy coming from the Sun. Other heat sources like heat Earth radiation (IR) and Albedo are negligible. Because of that, the entire external surface of the spacecraft ($50,14\text{ m}^2$) is covered by 40 layers MLI single goldized Kapton insulation [1]. The thermal requirements for electronics are given by the critical lower and upper limit temperature of -10°C and 50°C , respectively. To stabilize temperatures for optical instrumentation the Thermal Control System is composed of a conductive bridge, a MLI insulation, heaters, and a radiation dissipation surface. We chose a passive cooling installation consisting of a radiator surface and a Conductive Link that is made of annealed pyrolytic graphite. In order to dissipate $7,45\pm 1,5\text{ W}$ of the heat from the optical instrumentation, a radiator with surface of about $0,66\text{ m}^2$ is installed on the eclipsed side of spacecraft. The below table lists the required thermal power of the respective instruments. In case of stand-by mode, heaters will remain active to keep all electronics within the allowed temperature window.

Critical Technology	TRL
Primary Mirror	3
Echelle Spectrograph	3
Optical Path Mirror	3
Polarimeter Aperature Plate	3-4
Baffles	4
Spectropolarimeter	4
Long Slit Spectrograph	4
MCP Detectors	5-6

Table 3: Estimated ESA Technology Readiness Levels of critical technologies for this mission.

6.8 Power

The required power from the solar arrays is $1,2\text{kW}$ at any time. The overall power consumption is achieved by two Triple-Junction GaInP/GaAs solar panels. For a solar cells efficiency of at least 28% a total panel surface of $8,2\text{m}^2$ is needed. Since the Quasi-Halo orbit around L_2 does not have any eclipses time during operation, no electrical storage is required. Nevertheless, 28V Lithium-Ion batterie cells shall keep the necessary subsystems active during the orbit transfer. The capacity of the batteries are approximately 52 A-h and have 80% depth of discharge. The PCDU controls and distributes the power accross the Spacecraft.

6.9 Data Handling & Communications

A requirement of the amount of date to be stored downlinked was derived from the instrumentation requirements and is at maximum 40Gbit per day. A data autonomy requirement of 3 days was set as and as such the on board data handling is required to have a minimum capacity of 120Gbit. Redundant on-board computers were specified as this is single point of failure.

With regards to downlink the data, a link budget was performed to define a system that is capable to downlink the 40Gbit during the 1.5 hour daily downlink period. Assuming use of the 15m ESTRACK ground station in the X band, a 0.5m diameter high gain antenna and a transponder RF power of 30W is required. The antenna is fixed and as such the spacecraft must be pointed as a whole in order to downlink. S Band Low Gain Antennas are provided for TTC at other times.

7 Risk Management

Since this mission is based heavily off modified heritage systems, such as Hubble, Herschel, WUPPE, and Chandra, the technologies are not revolutionary. However, it is still of utmost importance to identify the

areas of high risk and propose mitigation techniques. The level of risk of a component can be ranked using the table shown in Figure 7. Our main risk drivers are the rotating mirror and the polarimeter plate mechanism. Both of these require a mechanism (a moving part) to work, which always introduces more likelihood of failure. The rotating mirror, responsible for directing the incoming light from the telescope into the desired instrument, would be a very serious failure. However, to mitigate this possibility of failure, the "rotation" can be discrete, such that the mirror must point only in the direction of an instrument and nowhere in between. In addition, the payload will be launched with the mirror arranged so it directs light into the Long Slit Spectrograph, since we can get the widest range of observations through this instrument. The polarimeter place is also a mechanism and has a higher-than-nominal chance of failure. This risk can be mitigated in a similar way to the rotating mirror. The payload can be launched with this aperture fixed at 2" and only rotate in discrete intervals to preserve at least minimal functionality.

Description	Thermal energy	Unit
Batteries heaters	70,000	W
Low Res Imager	20,000	W
Others instruments	50,000	W
Total heaters power	140,000	W

Figure 6: some awesome caption

8 Costs

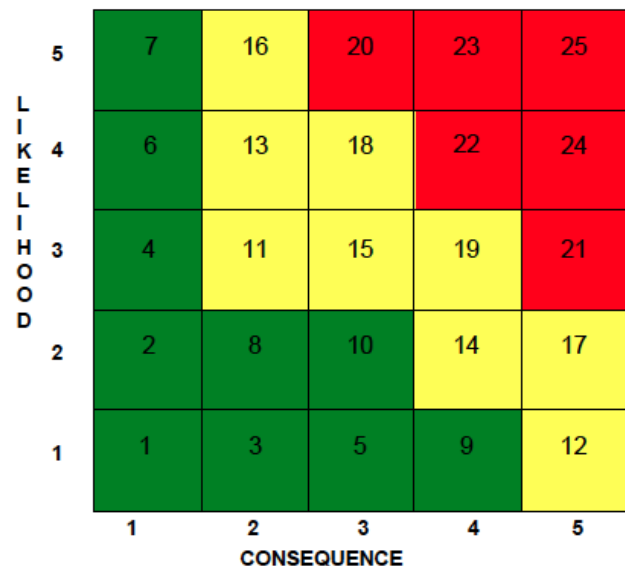
A cost breakdown was performed using a parametric costing method which took into account the mass, technological complexity index and specific cost of individual subsystems. Important factors were that a Soyuz dedicated launch will be used to take the mission to a Lagrangian orbit (L_2) with a mission duration of 5+ years, the telescope's diameter of 2 meters and Si-C structure and finally the fact that the MCPs will be Heritage from GALEX led to a final estimated cost of 825 M€.

9 Descoping Options

Two main options for descoping this mission have been identified and are described below.

- **Decrease Primary Mirror Size** : If the primary mirror size is reduced from 2 m to 1 m, the entire mission would be scaled down. This particular descoping would allow us to use a solid mirror, which would lift up the TRL level and coincidentally the cost of our payload (currently a cost driver). However, this would require a longer integration time, lower signal to noise ratio, and a survey that would be biased towards brighter pre-main sequence objects which could skew the scientific results.

Figure 7: Risk quantification diagram. The x axis represents the consequence, 5 being a complete mission failure. The y axis depicts the likelihood of a failure to occur. The ranking 1 is less than 20% chance that the failure will occur while 5 means $\geq 80\%$ chance of occurrence. The color scheme represented the severity and urgency of mitigation needs.



- **Dual Launch to SSO with Soyuz** : By selecting a Sun Synchronous Orbit (SSO), the Soyuz mass to orbit is increased enough to take two satellites of approximately our size to orbit. This would allow a cost sharing between the two missions, greatly reducing the launch costs. However, SSO is not the ideal orbit for this mission. In order to share a launch, the spacecraft would have to decrease in length by 0.5 m which would most likely come from shortening the baffles, allowing more stray light into our space craft. The pointing requirements are much more strenuous, allowing for only 30 minutes of integration time per target and significantly increased delta v.
- **Excluding 1 or more instruments** : Finally, it has been considered to exclude an instrument due to complexity. However, the science case would be fatally compromised if this were done. All four instruments are necessary to carry out a successful scientific mission.

- [20] Herbst, W. et al., 1994, AJ, 108 5, 1906
- [21] Gullbring, A. et al., 1994, A&A, 314, 835
- [22] Errico, L. et al., 2001, A&A, 377, 557
- [23] D'Alessio, P. et al., 1999, ApJ, 527, 893
- [24] Muzerolle, J. et al., 1994, ApJ, 426, 669

References

- [1] Schroeder, D. J. and Anderson, C. M. 1970, BAAS, vol 2, 217
- [2] E. Wilkinson 1999, UC-Boulder, COS-11-0012
- [3] 1998, ESA Bulletin 95
- [4] Gomez de Castro, A. I. et al. 2003, in The Future of Cool-Star Astrophysics, vol 12, 40-49
- [5] France, K. et al. 2011, Apj, 734, 31+-
- [6] France, K. et al. 2011, Apj, 729, 7-+
- [7] Prochter, G. E et al. 2006, ApjL, 648, L93-L96
- [8] Berdyugina, S. V. & Solanki, S. K 2001, 380, L5-L8
- [9] Errico, L., et al. 2001, A&A, 377, 557
- [10] Ward-Thompson & Whitworth, A.,P. *An Introduction to Star Formation*, Cambridge, 2011
- [11] Shu, F.H., et al. 1987, A&A, 377, 557
- [12] Lynden-Bell & Pringle L., 197, MNRAS (1974), 168, 603.
- [13] Calvet, N. & Hartmann, L., 1992, ApJ, 386, 239
- [14] Hartmann, L. et al., 1994, ApJ, 426, 669
- [15] Hartmann, L. et al., 1998, ApJ, 116, 2965
- [16] Hartmann, L. et al., 1994, ApJ, 116, 455
- [17] Muzerolle, J. et al., 1994, ApJ, 426, 669
- [18] Kenyon, S. et al., 1997, AJ, 108 5, 1872
- [19] Meyer, R. et al., 1997, AJ, 114 1, 288